DE GRUYTER
OPEN
10.1515/tvsb-2017-0033
Transactions of the VŠB – Technical University of Ostrava
Civil Engineering Series, Vol. 17, No. 2, 2017
paper #33

Stanislav SEITL[1], Petr MIARKA[2], Jakub SOBEK[3]

QUANTIFICATION OF INFLUENCE OF EPOXY LAYER BETWEEN INTERFACE STEEL-CONCRETE ON CALIBRATION CURVES FOR MODIFIED COMPACT TENSION TEST

Abstract

The objective of this study is to investigate the use of compact tension specimen calibration curves for evaluation data of fracture properties measurement performed on modified compact tension specimen made from cement based composites. From literature, the well-known calibration curve for compact tension specimen is compared with calibration curves for Modified compact tension specimen that are obtained from numerical calculation. The obtained results are quantified and accuracy of solution is discussed. The suggested curves could be preferably used for determining of the fracture parameters.

Keywords

Modified compact tension test, fracture, concrete, composite materials, load eccentricity, T-stress, calibration curves, test methods.

1. INTRODUCTION

Fracture in quasi-brittle heterogeneous materials such as: concrete, rock, cement based composites and bones, is characterised by the formation of a nonlinear zone ahead of a macroscopic crack in which energy is dissipated; which is defined as the Fracture Process Zone (FPZ) [4]. The size of this zone influences the load capacity of structures and is one of the parameters which determine a size effect on the nominal strength of structural members specific for quasi-brittle material sources. The FPZ could has various size and shape for different stress field in front of the crack that could influence determination of values of the fracture properties. Determination of the fracture properties of concrete is usually performed on common test configurations such as three-point bending or four point bending test with notch, see [17][18][5] [19], the another configuration is wedge splitting test (WST [27][21][15]), or wedge-splitting/bending test of notched specimens [29], CTS (compact tension shear) [9] [14][16], composite compact tension specimen [24] etc. [25].

In this paper, a numerical study of the stress field in specially shaped test specimens under combination of tensile and bending load (see Fig. 1) is introduced. The framework of Two-parameter fracture mechanics is kept for the study. Variations in eccentricity of tensile forces cause significant changes in the stress distribution in the tested specimens (thus the constraint of stress and deformation near the crack tip). An experimental campaign on sets of these modified specimens is under preparation in the laboratory at University of Sevilla. This contribution follows on and extends information given in [28], where numerical analysis of failure process (software ATENA with the cohesive crack modelling was used [7]) in specimens for this test configuration was done. The contribution also follows numerical calculations of calibration curves published in [22], where the interface of

[1] Assoc. Prof. Ing. Stanislav Seitl, Ph.D., Faculty of Civil Engineering, Brno University of Technology, Veveří 331/95, Brno 602 00, Czech Republic, phone: (+420) 541147361, seitl.s@fce.vutbr.cz.

[2] Ing. Petr Miarka, Faculty of Civil Engineering, Brno University of Technology, Veveří 331/95, Brno 602 00, Czech Republic, phone: (+420) 541147116, miarka.p@fce.vutbr.cz

[3] Ing. Jakub Sobek, Ph.D., Faculty of Civil Engineering, Brno University of Technology, Veveří 331/95, Brno 602 00, Czech Republic, phone: (+420) 541147116, sobek.j@fce.vutbr.cz

concrete/steel E_c = 40 GPa, E_s = 210 GPa is introduced, then the pilot study of concrete/steel interface influence (for E_c varied from 5 to 50 GPa) published in [23]. In order to provide a proper fracture mechanical evaluation of experimental data, it is necessary to known values of *COD* (Crack Opening Displacement – crack opening at the load-line), CMOD (Crack Mouth Opening Displacement), the *K*-calibration curve (stress intensity factor dependent on relative crack length), and constraint-calibration curve (generalized values of *T*-stress) for each relative crack length (*a*/*W*). The possible inaccuracy caused by material interface of calibration curves is discussed.

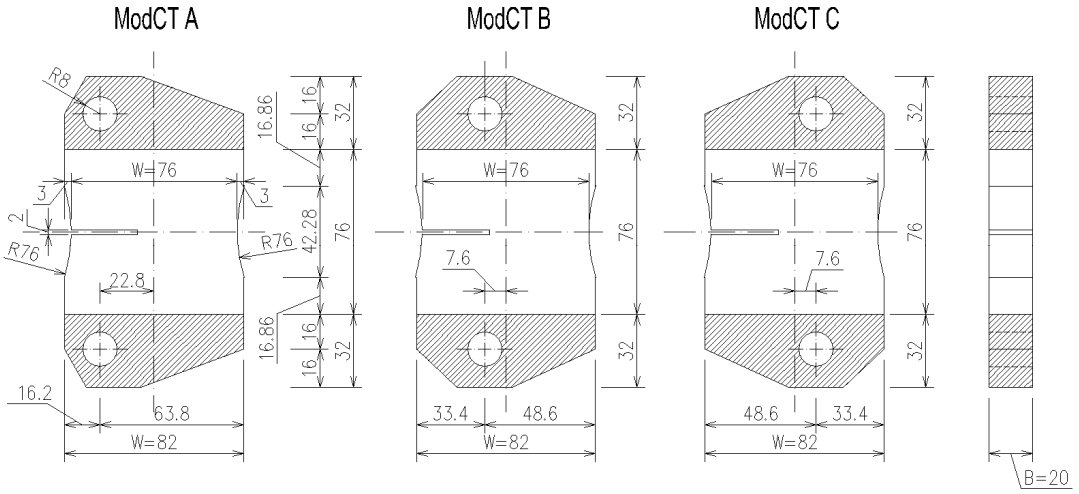

Fig.1: Studied configurations of ModCT test with glued loading plates and dog-bone shaped specimens with various position of load *P* (causes the change of the stress field in direction of the propagating crack), adopted from [28].

2. THEORETICAL BACKGROUND

2.1. Theory of Two-parameter fracture mechanics

In this paper, two-parameter constraint based on the Linear elastic fracture mechanics [13] is shown. Two terms of Williams expansion [30] are used to assess the constraint level at the crack tip. The in-plane constraint is characterized by the *T*-stress.

Elastic *T*-stress represents the normal stress acting parallel to the crack sides; it is related to the second (constant) term (following the first singular term) in the Williams expansion of the stress field in eq. (1). Practical application [21] and numerical calculations of *T*-stress can be found in [26][20][31]:

$$\sigma_{ij}(r,\theta) = \frac{K_I}{\sqrt{2\pi r}} f_{ij}^{I}(\theta) + T\delta_{1i}\delta_{1j}, \tag{1}$$

where

K_I – is stress intensity factor for loading mode I [MPam$^{1/2}$],

T – is *T*-stress [MPa],

δ – is Kronecker's delta [-],

r, θ – are radius and angle of polar coordinate system [m, rad].

$f^I_{ij}(\theta)$ – are known geometrical functions given by the Williams expansion [-].

2.2. Calibration curves of compact tension specimen

For fracture-mechanics evaluation of test results data, the knowledge of *K*, *T*-stress, *CMOD* and *COD* is necessary. For the standard compact tension (CT) specimen [2][25], which is similar to *ModCT A* configuration is given as polynomial function, see example for CT from handbook [25]:

$$K_{\mathrm{I}} = \frac{P\sqrt{a}}{B\,W}\frac{2(2+a/W)}{(1-a/W)^{3/2}}\frac{1}{\sqrt{a/W}}\begin{pmatrix}0.443 + 2.32(a/W) - 6.66(a/W)^2 + \\ 7.36(a/W)^3 - 2.8(a/W)^4\end{pmatrix}, \quad (2)$$

$$COD = \frac{P}{BE}\left(\frac{1+a/W}{1-a/W}\right)^2\left[2.163 + 12.219\left(\frac{a}{W}\right) - 20.065\left(\frac{a}{W}\right)^2 - 0.9925\left(\frac{a}{W}\right)^3 + 20.609\left(\frac{a}{W}\right)^4 - 9.9314(\frac{a}{W})^5\right], \quad (3)$$

$$CMOD = \frac{P}{BE}\left(1 + \frac{0.25}{a/W}\right)\left(\frac{1+a/W}{1-a/W}\right)^2\left[1.6137 + 12.678\left(\frac{a}{W}\right) - 14.231\left(\frac{a}{W}\right)^2 - 16.61\left(\frac{a}{W}\right)^3 + 35.05\left(\frac{a}{W}\right)^4 - 14.494(\frac{a}{W})^5\right], \quad (4)$$

where:

a – is crack length [m],

W – is specimen width [m],

B – is thickness of specimen [m],

P – is load [N],

E – is Young's modulus [Pa].

3. NUMERICAL MODEL AND MATERIAL PROPERTIES

3.1. Model in ANSYS

Finite element models were created in ANSYS [1] finite element software by using PLANE 183 element type. These quarter-point crack tip elements take into account the crack tip singularity. The stress intensity factor (K) and T-stress for a particular loading and crack conditions were calculated with plane strain condition (assumption of the thickness higher than 20 mm against 76 mm height, but for numerical calculation the unit thickness of specimen is used). Details of calculation of the fracture parameters can be found in e.g. [21][22][23].

3.2. Material properties

In order to obtain the relevant calibration curves, a literature overview [6] of the material's properties was conducted. The range of real material properties is summarized in Table 1. Based on this data the theoretically possible intervals of the properties (Young's modulus E and Poisson's ratio ν) for the particular materials were selected as follows:

Concrete: $E \in \langle 5; 50\rangle$ GPa and $\nu = 0.2$,

Steel part: $E = 210$ GPa and $\nu = 0.3$,

Epoxy in layer $E = 4.75$ GPa and $\nu = 0.39$.

Tab.1: Range of Young's modulus and Poisson's ratio of the selected materials

Materials/Elastic properties	Young's modulus [GPa]	Poisson's ratio [–]
Foam concrete [10]	1÷8	
Concrete in [3]	30.6÷33.22	0.18÷0.21
High performance self-compacting concrete in [32]	30÷50	
Epoxy in [12]	4.75	0.39

4. NUMERICAL RESULTS AND DISCUSSION

Regular CT test [2] is loaded by the splitting component of the eccentrically imposed tensile force. Points of the applicate tensile load are placed in openings of the test specimen, namely in the drilled holes. Than the load is imposed through pins inserted into these openings. However, several problems come out in the case of quasi-brittle materials. And this is both with the creation of the openings (for input of the load device pins) and then with the actual loading of the specimens. During numerical simulations of the CT specimen [28] it has been found that failure occurs in the specimen at the contact of the opening and the pin imposing the load. Because of this reason, alternative ways, how to apply the tensile load to reach failure initiated exclusively from the notch, were sought. Considered configurations of modified CT test – differing in the way of the tensile load application directly through metal plates.

Fig. 1 shows the configuration where the upper and bottom side of the specimen (those that are perpendicular to the tensile force direction) are stiffened by glued steel part preventing the above-described failure; the way of imposing the load through the openings in the steel platen is kept without changes.

Several variants of different position of the applied tensile load and the crack length were considered to achieve differences in the fracture process zone properties. Letter A in the name of the variant indicates that a tensile load is applied closest to the edge of the modified CT specimen in which the notch is formed (eccentricity of tensile force is $0.3W' - W'$ is the specimen width in the narrower section, see Fig. 1 left). Variant B represents the load which resultant is closer to the axis of symmetry of the specimen from the notch side (eccentricity of $0.1W'$); and finally, in the C variant, the load resultant follows immediately after the symmetry axis (eccentricity of $0.1W'$). The notch length a (initial crack) was chosen at values of the ratio of $a/W' \in \langle 0.1; 0.9 \rangle$.

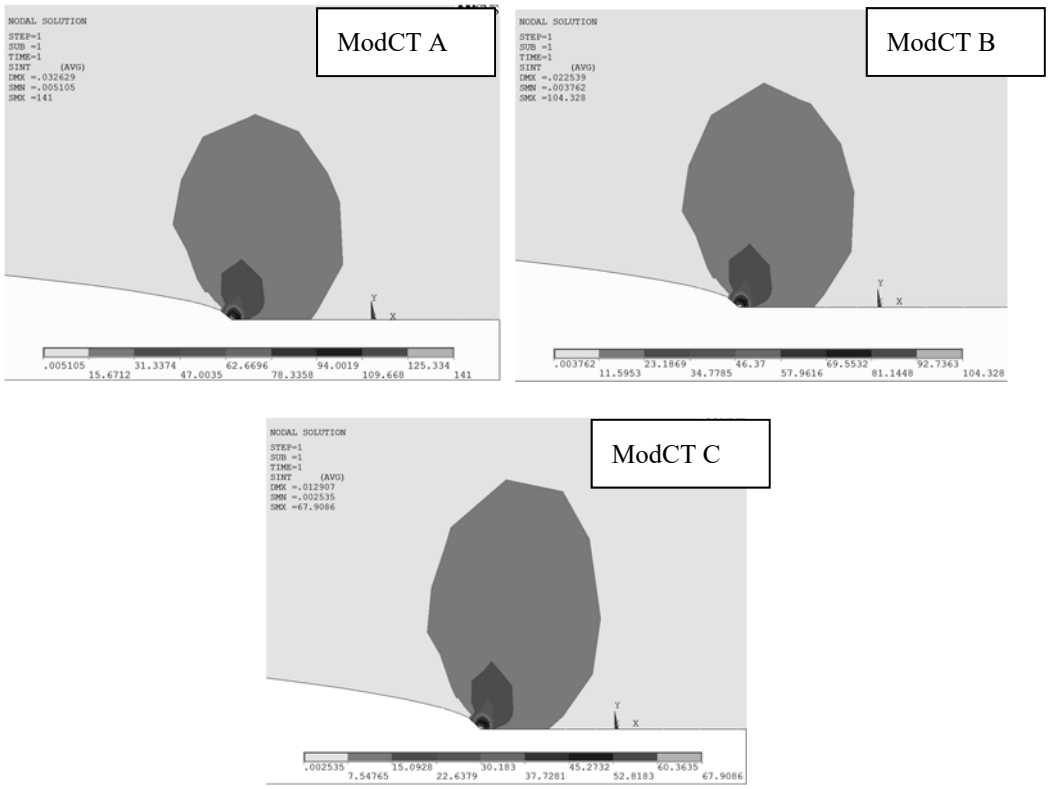

Fig. 2: Comparison of stress intensity field in front of the crack tip for $a/W = 0.4$, the same force $P = 100$ N, $E_c = 40$ GPa and various plate opening position A, B and C.

Fig. 2 shows the distribution of the stress intensity in front the crack tip (along the ligament) for crack length $a/W = 0.4$. It can be seen that stress profile and intensity changes with the load position. Thus, for evaluation of experimental data, the knowledge of calibration curves for each ModCT is necessary.

4.1. Comparison ModCT (A, B, C) with CT

Examples of the K and T-calibration curves of ModCT in variants A, B, and C for stress intensity factor corresponding to load $P = 100$ N and ratio $E_c/E_s = 5/210$, are shown in Fig. 3 where they can be compared with the curve for the standard CT specimen. The calibration curves exhibit a descending trend with the decreasing level of bending; it can be especially seen for the eccentricity C. We could conclude that for each variant we need the calibration curve.

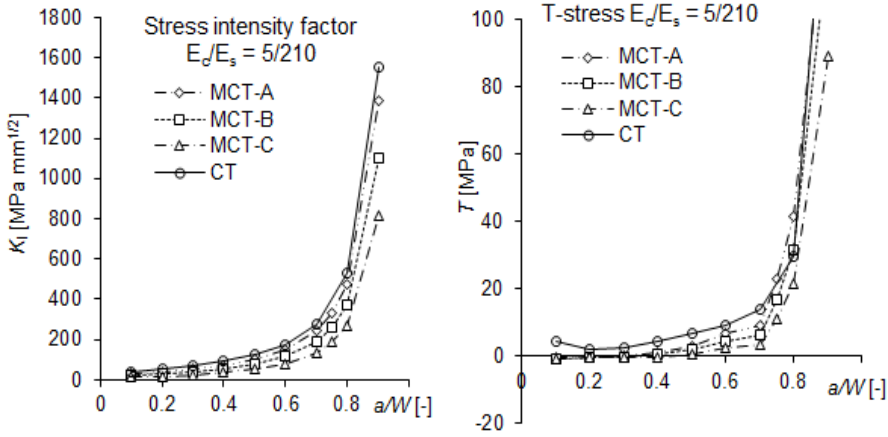

Fig. 3: For example, the K and T-calibration curves of ModCT for variants A, B, and C (see Fig. 1) for stress intensity factor corresponding to load $P = 100$ N and ratio $E_c/E_s = 5/210$.

Fig. 4 shows the adequate CT and ModCT curves for COD and CMOD versus relative crack length (a/W) for $W = 63.8$ mm. The materials properties are $E_c/E_s = 40/210$ [GPa/GPa = 1] and the applied load is 100 N.

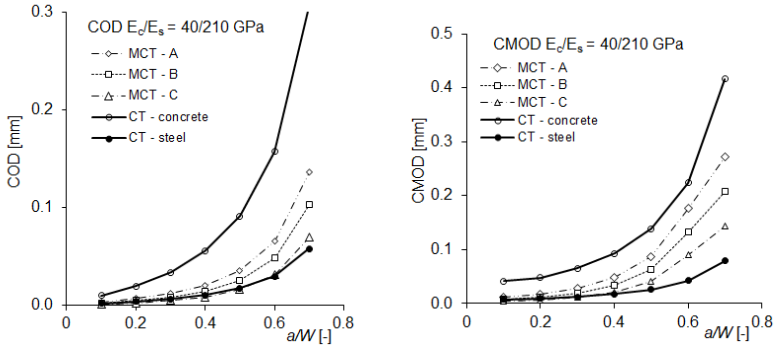

Fig. 4: COD and CMOD curves for studied variants of CT and ModCT specimens – load $P = 100$ N, for $E_c/E_s = 40/210$.

4.2. Influence of bi-material interface steel/concrete

The stress intensity factor K_I and T-stress progress as a function of the relative crack length (a/W) has practically the same values for all study cases of Mod CT, see Fig. 5 and 6. Thus, the same calibration curves could be used for all cases of ModCT. This means that the use of steel plates has not an influence on the ModCT calibration curve for stress intensity factor K_I and T-stress.

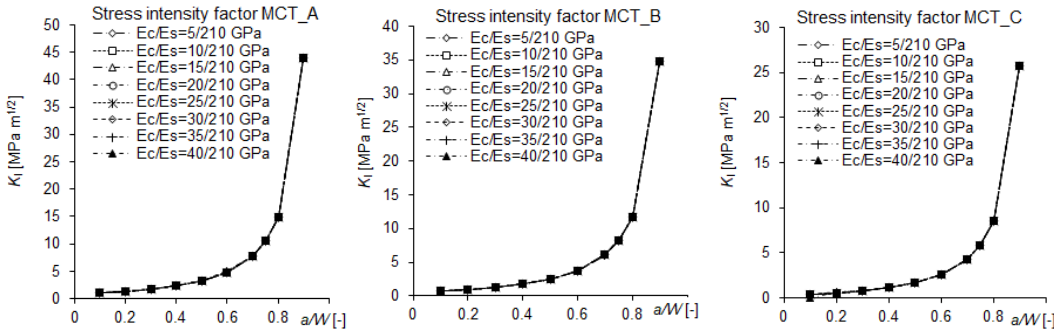

Fig. 5: The values of stress intensity factor for ModCT variants A, B, C for various ratio of concrete/steel Young's modulus, the applied load is 100 N.

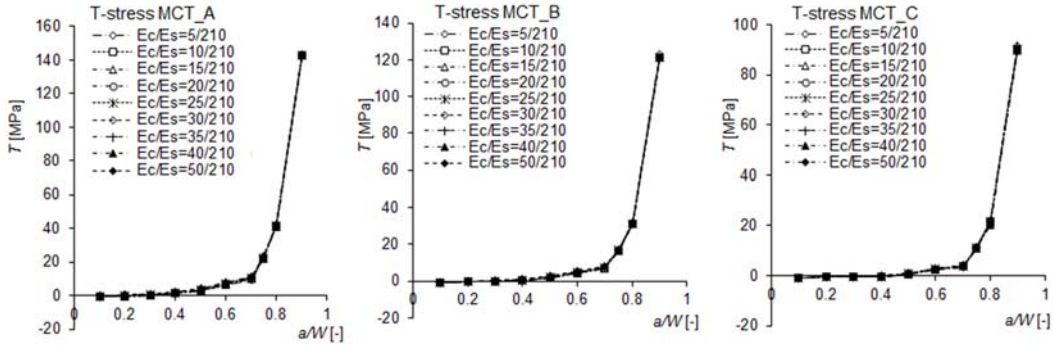

Fig. 6: The values of *T*-stress for Mod CT variants A, B, C for various ratio of concrete/steel Young's modulus, the applied load is 100 N.

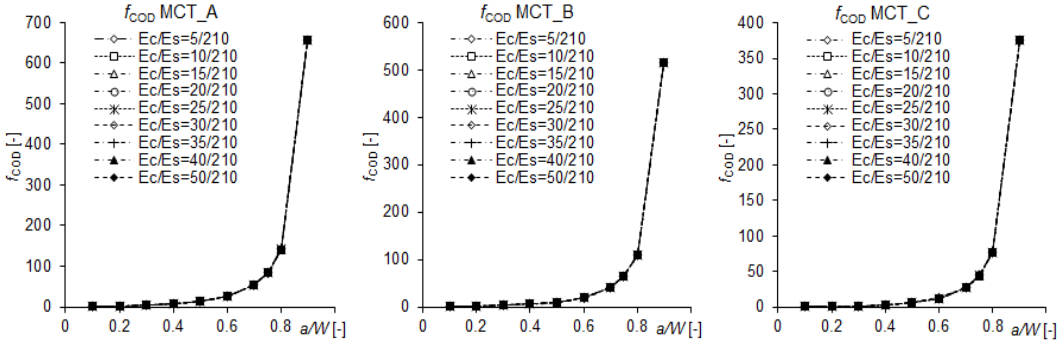

Fig. 7: The values of COD function for ModCT variants A, B, C for various ratio of concrete/steel Young's modulus.

4.3. Influence of epoxy layer

The concrete part and steel part has to be glued together. For numerical study, epoxy inlayer size between concrete and steel, was taken as additional 2 mm layer with following materials properties of the epoxy inlayer: Young's modulus $E = 4.75$ GPa and Poisson's ratio $\nu = 0.39$. The influence of the epoxy layer on calibration curves is quantified by deviation of the SIF and COD values.

For quantification of the error caused by the various kinds of material, the graphs of maximal deviation between the homogeneous specimen and the steel plates and the epoxy part are plotted in Fig. 9. The figure shows deviation in interval of $0.3 \leq a/W \leq 0.8$. The error is up to 10 % and it is impossible to neglect it in the evaluation of the fracture parameters (e.g. fracture energy, etc.).

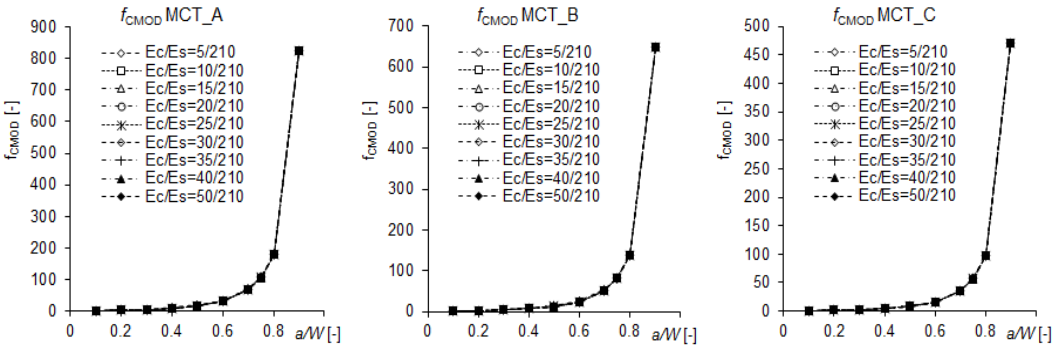

Fig. 8: The values of CMOD function for ModCT variants A, B, C for various ratio of concrete/steel Young's modulus.

4.4. Recommended calibration curves

In this paragraph, the recommended calibration curves for evaluation of data from the experiment are mentioned in following form:

$$K_I = \sigma\sqrt{a} f_I, \tag{5}$$

where

$$\sigma = \frac{P}{WB}, \tag{6}$$

$$f_I(A) = \frac{2(2+a/W)}{(1-a/W)^{3/2}\sqrt{a/W}}\left[0.5679 + 0.296\left(\frac{a}{W}\right) - 0.3944\left(\frac{a}{W}\right)^2 + 0.2849\left(\frac{a}{W}\right)^3 - 0.00961\left(\frac{a}{W}\right)^4\right], \tag{7}$$

$$f_I(B) = \frac{2(2+a/W)}{(1-a/W)^{3/2}\sqrt{a/W}}\left[0.3768 + 0.323\left(\frac{a}{W}\right) - 0.2159\left(\frac{a}{W}\right)^2 + 0.0065\left(\frac{a}{W}\right)^3 + 0.0398\left(\frac{a}{W}\right)^4\right], \tag{8}$$

$$f_I(C) = \frac{2(2+a/W)}{(1-a/W)^{3/2}\sqrt{a/W}}\left[0.1949 + 0.3289\left(\frac{a}{W}\right) - 0.0707\left(\frac{a}{W}\right)^2 - 0.1603\left(\frac{a}{W}\right)^3 + 0.1068\left(\frac{a}{W}\right)^4\right]. \tag{9}$$

For the curve of *T*-stress, the following formulas could be used:

$$T = \frac{B_2 K_I}{\sqrt{\pi a}}, \tag{10}$$

where

$$B_2(A) = -0.3126 + 2.5893\left(\frac{a}{W}\right) - 5.6196\left(\frac{a}{W}\right)^2 + 5.806\left(\frac{a}{W}\right)^3, \tag{11}$$

$$B_2(B) = -0.3939 + 2.5701\left(\frac{a}{W}\right) - 5.6598\left(\frac{a}{W}\right)^2 + 5.9586\left(\frac{a}{W}\right)^3, \tag{12}$$

$$B_2(C) = -0.4521 + 1.8615\left(\frac{a}{W}\right) - 4.1085\left(\frac{a}{W}\right)^2 + 5.108\left(\frac{a}{W}\right)^3. \tag{13}$$

For evaluation of data from COD measurement, the following formulas could be used:

$$COD = \frac{P}{E_c} f_{COD}\left(\frac{a}{W}\right), \tag{14}$$

where

$$f_{COD}(A) = \left(\frac{1+a/W}{1-a/W}\right)^2 (0.138 + 2.1653(a/W) - 7.734\left(\frac{a}{W}\right)^2 + 17.134\left(\frac{a}{W}\right)^3 - 21.67\left(\frac{a}{W}\right)^4 + 14.743\left(\frac{a}{W}\right)^5 - 4.2075\left(\frac{a}{W}\right)^6), \tag{15}$$

$$f_{COD}(B) = \left(\frac{1+a/W}{1-a/W}\right)^2 (0.0926 + 1.4645\left(\frac{a}{W}\right) - 5.0604\left(\frac{a}{W}\right)^2 + 11.368\left(\frac{a}{W}\right)^3 - 14.41\left(\frac{a}{W}\right)^4 + 9.7911 - 2.7877\left(\frac{a}{W}\right)^6), \tag{16}$$

$$f_{COD}(C) = \left(\frac{1+a/W}{1-a/W}\right)^2 (0.0485 + 0.7874\left(\frac{a}{W}\right) - 2.489\left(\frac{a}{W}\right)^2 5.7333\left(\frac{a}{W}\right)^3 - 7.1762\left(\frac{a}{W}\right)^4 + 4.7739\left(\frac{a}{W}\right)^5 - 1.3311\left(\frac{a}{W}\right)^6), \quad (17)$$

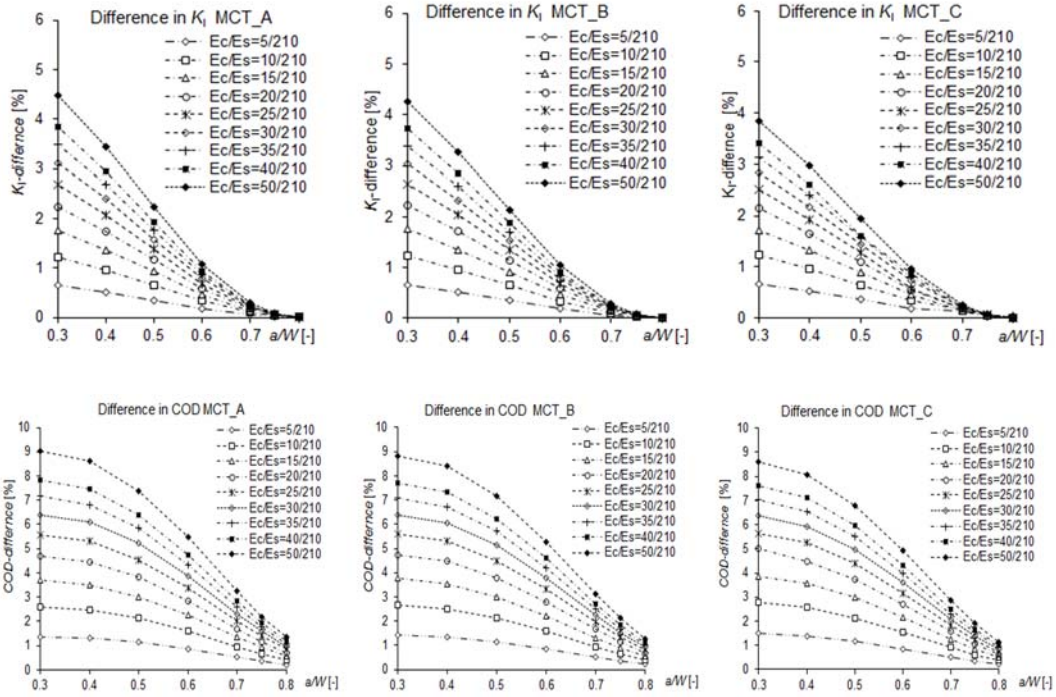

Fig. 9: The maximal percentual difference for various ModCT: a) stress intensity factor, b) COD

and for evaluation of data from CMOD measurement, the following formulas could be used:

$$CMOD = \frac{P}{E_c} f_{CMOD}\left(\frac{a}{W}\right), \quad (18)$$

where

$$f_{CMOD}(A) = \left(1 + \frac{0.25}{a/W}\right)\left(\frac{1+\frac{a}{W}}{1-\frac{a}{W}}\right)^2 (0.5128 + 2.681\left(\frac{a}{W}\right) - 0.3216\left(\frac{a}{W}\right)^2 - 1.0722\left(\frac{a}{W}\right)^3 + 7.6266\left(\frac{a}{W}\right)^4 - 9.1648\left(\frac{a}{W}\right)^5 + 3.4026\left(\frac{a}{W}\right)^6), \quad (19)$$

$$f_{CMOD}(B) = \left(1 + \frac{0.25}{a/W}\right)\left(\frac{1+\frac{a}{W}}{1-\frac{a}{W}}\right)^2 (0.3332 + 1.823\left(\frac{a}{W}\right) - 0.0515\left(\frac{a}{W}\right)^2 + 0.0804\left(\frac{a}{W}\right)^3 + 4.2804\left(\frac{a}{W}\right)^4 - 5.7475\left(\frac{a}{W}\right)^5 + 2.21\left(\frac{a}{W}\right)^6), \quad (20)$$

$$f_{CMOD}(C) = \left(1 + \frac{0.25}{a/W}\right)\left(\frac{1+\frac{a}{W}}{1-\frac{a}{W}}\right)^2 (0.1632 + 0.9215\left(\frac{a}{W}\right) + 0.7125\left(\frac{a}{W}\right)^2 - 0.7451\left(\frac{a}{W}\right)^3 + 4.3781\left(\frac{a}{W}\right)^4 - 5.1457\left(\frac{a}{W}\right)^5 + 1.9118\left(\frac{a}{W}\right)^6). \quad (21)$$

From the knowledge of the applied loading force *P*, crack length *a* and introduced numerical study for ModCT, the following fracture properties could be determined:

- for double-*K* fracture criteria [8] – initial fracture toughness and the failure fracture toughness
- equivalent elastic fictitious crack etc. see in [11].

CONCLUSION

A finite element analysis of the ModCT of various specimen configurations was performed by means of a constraint-based two parameter fracture mechanics approach. Three different specimen configurations ModCT A, B, C were investigated. The following conclusions could be derived:

- The influence of the specimen configurations on the calibration curves' values is negligible and the same polynomial function covers all three cases. The possible mistake/deviation of the results is smaller than 1.5 %.
- The influence of the configuration ModCT A, B, C on the calibration curves' values for stress intensity factor is not negligible and different polynomial function has to be used, see paragraph 4.4.

ACKNOWLEDGMENT

This paper has been worked out under the "National Sustainability Programme I" project "AdMaS UP – Advanced Materials, Structures and Technologies" (No. LO1408) supported by the Ministry of Education, Youth and Sports of the Czech Republic.

LITERATURE

[1] ANSYS, Finite element software www.ansys.com

[2] ASTM – Standard test method for measurement of fatigue crack growth rates, E 647–99, ASTM, 100 Barr Harbor Drive, West Conshohocken, PA 19428-2959, United States.

[3] BAHR, O. SCHAUMANN, P. BOLLEN, B. & BRACKE, J. Young's modulus and Poisson's ratio of concrete at high temperatures: Experimental investigations. *Materials and Design.* 2013, 45, pp. 421–429. ISSN 0264-1275.

[4] BAŽANT, Z.P. *Scaling of Structural Strength*. Second edition, Elsevier. 2005, 340 pp. ISBN 0-7506-6849-0.

[5] BÍLEK(Jr), V. ŠIMONOVÁ. H. HAVLÍKOVÁ, I. TOPOLÁŘ, l. KUCHARCZYKOVÁ, B. & KERŠNER, Z. Alkali activated binders based concrete specimens: Length change and fracture tests. *Solid State Phenomena.* 2017, 258, pp. 623–626. ISSN 16629779.

[6] BORESI, A. P. SCHMIDT, R. J. & SIDEBOTTOM, O. M. *Advanced Mechanics of Materials.* Wiley. 2003, 700 pp. ISBN 978-0-471-43881-6.

[7] ČERVENKA, V. ČERVENKA, J. & PUKL, R. ATENA - A tool for engineering analysis of fracture in concrete. *Proceedings in Engineering Sciences.* 2002, 27, pp. 485–492.

[8] HAVLÍKOVÁ, I. MAJTÁNOVÁ, R.V. ŠIMONOVÁ, H. LÁNÍK, J. & KERŠNER, Z. Evaluation of three-point bending fracture tests of concrete specimens with polypropylene fibres via double-K model. *Key Engineering Materials*. 2014, 592-593, pp. 185–188.

[9] HORNÍKOVÁ, J. ŽÁK, S. & ŠANDERA, P. Numerical Fracture Analysis of Compact Tension Shear (CTS) Specimens with Tortuous Crack Fronts. *Key Engineering Materials*. Trans Tech Publications, 2016. pp. 77–80. ISSN 1013-9826.

[10] JONES, M. R. & MCCARTHY. A, Preliminary views on the potential of foamed concrete as a structural material. *Magazine of Concrete Research.* 2005, 57, pp. 21–31, ISSN 0024-9831.

[11] KARIHALOO, B.L. *Fracture Mechanics and Structural Concrete*. Longman Scientific & Technical, 330 pp. Harlow, UK, 1995.

[12] KLUSÁK, J. HELINCKS. P. SEITL, S. De CORTE, W. BOEL, V. & De SCHUTTER, G. The influence of the epoxy interlayer on the assessment of failure conditions of push-out test specimens. *Key Engineering Materials.* 2013, Vols. 525-526, pp. 61–64. ISSN 1662-9795.

[13] LEEVERS, P. S. & RADON, J. C. Inherent stress biaxiality in various fracture specimen geometries. *International. Journal of Fracture*. 1982, Nr. 19, pp. 311–325.

[14] MA, S. YHANG, X.B. RECHO, N. & LI, J. The mixed-mode investigation of the fatigue crack in CTS metallic specimen. *International Journal of Fatigue*. 2006, Nr. 28(12), pp. 1780–1790.

[15] MERTA, I. & TSCHEGG, E. K. Fracture energy of natural fibre reinforced concrete. *Construction and Building Materials*. 2013, Nr. 4, pp. 991–997. ISSN 0950-0618.

[16] PEIXOTO, D. F. C. & DE CASTRO, P. M. S. T. Mixed mode fatigue crack propagation in railway wheel steel. *Procedia Structural Integrity.* 2016, Nr. 1, pp. 150–157. ISSN 2452-3216.

[17] RILEM TC 50-FMC. Determination of the fracture energy of mortar and concrete by means of three-point bend test on notched beams. *Material and Structures.* 1985, 18, pp. 285–290.

[18] SHAH, S. P. & CARPINTERI, A. (eds.). *Fracture Mechanics Test Methods for Concrete*. RILEM Report 5. 1991, 400 pp. Chapman & Hall, London. ISBN 1-412-41100-8

[19] ROVNANÍK, P. ŠIMONOVÁ, H. TOPOLÁŘ, L. SCHMID, P. & KERŠNER, Z. Effect of carbon nanotubes on the mechanical fracture properties of fly ash geopolymer. *Procedia Engineering.* 2016, 151, pp. 321–328.

[20] SEITL, S. & VISZLAY, V. Modified compact tension specimen for experiments on cement based materials: comparison of calibration curves from 2D and 3D numerical solutions. *Frattura ed Integrità Strutturale*. 2017, 39, pp. 118–128. ISSN 1971-8993.

[21] SEITL, S. NIETO GARCIA, B. & MERTA, I. Wedge splitting test method: Quantification of influence of blues marble plates by two-parameter fracture mechanics. *Frattura ed Integrita Strutturale*. 2014, 30, pp. 174–181. ISSN 1971-8993, DOI: 10.3221/IGF-ESIS.30.23.

[22] SEITL, S. RÍOS, J. D. CIFUENTES, H. & VESELÝ, V. Effect of the Load Eccentricity on Fracture Behaviour of Cementitious Materials Subjected to the Modified Compact Tension Test. *Solid State Phenomena*. 2017, 258, pp. 518–521. ISSN 1662-9779.

[23] SEITL, S. & MIARKA, P. Quantification of influence of material interface steel-concrete on calibration curves for modified compact tension test. *Modelling in Mechanics* 2017. Ostrava 2017, on CD, pp. 8. ISBN 978-80-248-4010-9.

[24] SLEEPETZ, J. M., & CARLSON, L. Fracture of Composite Compact Tension Specimens. *American Society for Testing and Materials*. 1975, pp. 143–165.

[25] TADA, H. PARIS, P. C. & IRWIN, G. R. *The stress Analysis of Cracks Handbook*, New York. ASME Press, 2000, 677 pp. ISBN 1-86058-304-0.

[26] TAN, C. L. & WANG, X. The use of quarter-point crack-tip elements for *T*-stress determination in boundary element method analysis. *Engineering Fracture Mechanics.* 2003, Nr. 70, pp. 2247–2252.

[27] TSCHEGG, E.K. *Equipment and appropriate specimen shapes for tests to measure fracture values*. Austrian Patent AT No. 390328, 1986,Austrian Patent Office, Austria.

[28] VESELÝ, V. & SOBEK. J. Numerical study of failure of cementitious composite specimens in modified compact tension fracture test. *Transactions of the VŠB-Technical University of Ostrava*, 13(2) 2013, *Civil Engineering Series*, paper #25, DOI: 10.2478/tvsb-2013-0025.

[29] VESELÝ, V. MERTA, I. ŠIMONOVÁ, H. SCHNEEMAYER, A. SEITL, S. & KERŠNER, Z. Component wedge-splitting/bending test of notched specimens enforcing various crack-tip constraint conditions: Experiments and simulations, *9th International Conference on Fracture Mechanics of Concrete and Concrete Structures FraMCoS-9*, 2016,

[30] WILLIAMS, M. L. On the stress distribution at the base of a stationary crack. *ASME Journal of Applied. Mechanics*, 1957, Nr. 24, pp. 109–114.

[31] YANG, B. & RAVI-CHANDAR, K. Evaluation of elastic *T*-stress by the stress difference method. *Engineering. Fracture Mechanics*. 1999, Nr. 64, pp. 589–605.

[32] YURTDAS, I. BURLION, N. SHAO, J. F. & LI, A. Evolution of the mechanical behaviour of a high performance self-compacting concrete under drying. *Cement & Concrete Composites.* 2011, 33, pp. 380–388. ISSN 0958-9465